

# Revisiting the linear stability analysis and absolute–convective transition of two fluid core annular flow

D. Salin<sup>1,†</sup> and L. Talon<sup>1</sup>

<sup>1</sup>Laboratoire FAST, Univ Paris-Sud, CNRS, Université Paris-Saclay, F-91405, Orsay, France

(Received 10 August 2018; revised 23 November 2018; accepted 18 January 2019)

Numerous experimental, numerical and theoretical studies have shown that core annular flows can be unstable. This instability can be convective or absolute in different situations: miscible fluids with matched density but different viscosities, creeping flow of two immiscible fluids or buoyant flow along a fibre. The analysis of the linear stability of the flow equation of two fluids injected in a co-current and concentric manner into a cylindrical tube leads to a rather complex eigenvalue problem. Until now, all analytical solution to this problem has involved strong assumptions (e.g. lack of inertia) or approximations (e.g. developments at long or short wavelengths) even for axisymmetric disturbances. However, in this latter case, following C. Pekeris, who obtained, almost seventy years ago, an elegant explicit solution for the dispersion relationship of the flow of a single fluid, we derive an explicit solution for the more general case of two immiscible fluids of different viscosity, density and inertia separated by a straight interface. This formulation is well adapted to commercial software. First, we review the creeping flow limit (zero Reynolds number) of two immiscible fluids as it is used in microfluidics. Secondly, we consider the case of two fluids of different viscosities but of the same density in the absence of surface tension and also without diffusion (i.e. miscible fluids with infinite Schmidt number). In both cases, we study the transition from convective to absolute instability according to the different control parameters.

**Key words:** absolute/convective instability, core-annular flow

---

## 1. Introduction

Following the pioneering theoretical work of Hickox (1971), the hydrodynamic stability of two-phase flows in a pipe has been extensively studied, experimentally, numerically and theoretically (Joseph, Renardy & Renardy 1984; Hu & Joseph 1989; Joseph & Renardy 1992*a,b*; Joseph *et al.* 1997; Kouris & Tsamopoulos 2002; Sahu *et al.* 2009; Selvam *et al.* 2009; Govindarajan & Sahu 2014). These studies have improved the understanding of the stability of parallel shear flows. Over the past decades, the issue of the convective or absolute nature of this instability (Briggs 1964; Huerre & Monkewitz 1990) has been addressed in different contexts. In hydrodynamic

<sup>†</sup> Email address for correspondence: [salin@fast.u-psud.fr](mailto:salin@fast.u-psud.fr)

open flows, this transition from a convective instability to an absolute one has been discovered in wakes and jets (Chomaz 2005), in thin film falling along a tilted wall (Brevdo, Laure & Bridges 1999) or on a fibre (Duprat *et al.* 2007). In this latter case, the control parameters are capillarity, inertia and geometry. In microfluidics, the need to provide calibrated droplets on demand has led to the design of micro capillary co-flow and flow-focusing devices (Gañán-Calvo, Herrada & Garstecki 2006; Utada *et al.* 2007; Hu & Cubaud 2018) in which the break-up of the liquid jet into droplets has been accounted for by the transition from a convective instability to an absolute one (Guillot *et al.* 2007; Guillot, Colin & Ajdari 2008; Herrada, Gañán Calvo & Guillot 2008; Utada *et al.* 2008). In the latter case, viscous and capillary effects are involved. In neutrally buoyant miscible core annular parallel flows, thus in the absence of interfacial tension, a convective/absolute transition has been observed (d'Olce *et al.* 2009) and analysed numerically (Selvam *et al.* 2009) as a function of the control parameters, namely the viscosity ratio of the two fluids, the inertia and the location of the pseudo-interface. It should be noted that, in such core annular flow, the threshold of the transition between pearl and mushroom patterns (d'Olce *et al.* 2008), analogous to the dripping/jetting transition for immiscible fluids, does not correspond to the threshold of the convective/absolute transition.

However, when buoyancy is present, the instability may lead to non-axisymmetric patterns such as corkscrew, snake, bamboo etc. (Joseph & Renardy 1992*a,b*; Lajeunesse *et al.* 1999; Balasubramaniam *et al.* 2005). Without buoyancy, the observed instability patterns are axisymmetric in both experiments (Petitjeans & Maxworthy 1996; Gañán-Calvo *et al.* 2006; Duprat *et al.* 2007; Utada *et al.* 2007; d'Olce *et al.* 2008, 2009) and numerical simulations (Chen & Meiburg 1996; Kouris & Tsamopoulos 2001, 2002; Kuang, Maxworthy & Petitjeans 2003; Gañán-Calvo *et al.* 2006; Guillot *et al.* 2007; Selvam *et al.* 2007; Guillot *et al.* 2008; Utada *et al.* 2008; Selvam *et al.* 2009). Moreover in Selvam *et al.* (2007), it was shown that the axisymmetric mode is dominant over the non-axisymmetric corkscrew one for large enough Schmidt numbers (ratio of viscous to molecular diffusivities) which is the case for most experimental fluids. Therefore, a linear stability analysis (LSA) can be performed assuming only axisymmetric disturbances of the core annular parallel flow. This is of course a tremendous simplification. The LSA requires us both to calculate, from the Navier–Stokes equation, the flow perturbations in the bulk of each fluid and to match the boundary conditions at the interface of the two fluids. Here, thanks to the axisymmetric geometry of the problem, we can extend the single-phase bulk solution of Pekeris (1948) to the two-phase core annular flow. We determine the bulk solution for each fluid using Bessel and confluent hypergeometric functions. Using these two bulk solutions and matching the boundary conditions at the interface between the two fluids allows us to solve the eigenvalue problem explicitly. First we revisit the creeping flow limit ( $Re = 0$ ) for two immiscible fluids. We also address the transition from a convective instability to an absolute one, as was used in microfluidic devices to account for the transition from dripping to jetting. Then, using the general solution, we study the stability of two fluids with different viscosities but with the same density in the absence of an interfacial tension; this situation is equivalent to the pseudo-interface between two miscible fluids without diffusion (infinite Schmidt number) which allows us to compare our results with the miscible fluids study of Selvam *et al.* (2007, 2009). We determine the convective or absolute nature of the instability as a function of the Reynolds number,  $Re$ , or the interface location  $h$ .

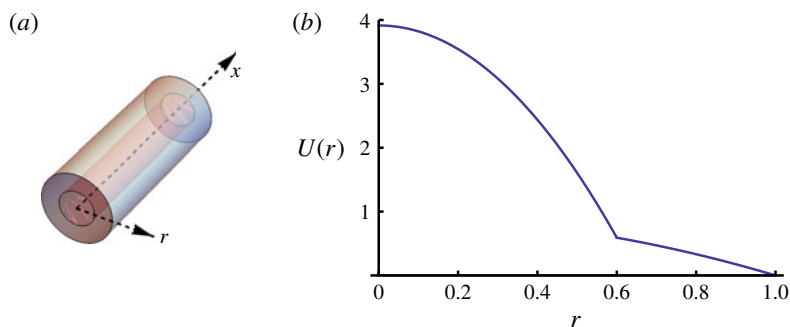


FIGURE 1. (Colour online) (a) Sketch of the core annular parallel flow geometry, with different colours for the core and the wall fluids. The  $x$  axis is the symmetry axis of the cylinder; the radial axis is normal to it. (b) Dimensionless velocity versus the dimensionless radius  $r$ . The dimensionless position of the interface is  $h = R_s/R = 0.6$  and the viscosity ratio of the two fluids is  $M = 10$ .

## 2. Governing equations

We consider the flow of two incompressible fluids of different viscosity and density in the absence of buoyancy. The fluids are injected co-currently and concentrically (see figure 1) into a cylindrical pipe of radius  $R$ . A straight interface separates the two fluids at the radial position  $R_s$ . The base flow is axisymmetric (Joseph & Renardy 1992*a,b*). Moreover, since the observed instability patterns are also axisymmetric in both experiments and numerical simulations (Gañán-Calvo *et al.* 2006; Duprat *et al.* 2007; Guillot *et al.* 2007; Selvam *et al.* 2007; d'Olce *et al.* 2008; Utada *et al.* 2008; d'Olce *et al.* 2009; Selvam *et al.* 2009), we will also assume axisymmetric perturbations. Therefore, the Navier–Stokes equation in cylindrical polar coordinates  $(x, r, \varphi)$ , for axisymmetric flow ( $v_\varphi = 0$ ,  $\partial/\partial\varphi = 0$ ), can be reduced to the radial  $v_r(x, r, t)$  and the axial  $v_x(x, r, t)$  components of  $\mathbf{v}(v_x, v_r)$ :

$$\rho_l \left( \frac{\partial v_x}{\partial t} + v_r \frac{\partial v_x}{\partial r} + v_x \frac{\partial v_x}{\partial x} \right) = -\frac{\partial p}{\partial x} + \mu_l \left[ \frac{\partial^2 v_x}{\partial r^2} + \frac{1}{r} \frac{\partial v_x}{\partial r} + \frac{\partial^2 v_x}{\partial x^2} \right], \quad (2.1)$$

$$\rho_l \left( \frac{\partial v_r}{\partial t} + v_r \frac{\partial v_r}{\partial r} + v_x \frac{\partial v_r}{\partial x} \right) = -\frac{\partial p}{\partial r} + \mu_l \left[ \frac{\partial^2 v_r}{\partial r^2} + \frac{1}{r} \frac{\partial v_r}{\partial r} - \frac{v_r}{r^2} + \frac{\partial^2 v_r}{\partial x^2} \right], \quad (2.2)$$

where  $p$  is the pressure,  $l = 1$  for the core fluid ( $0 \leq r \leq r_i$ ) and  $l = 2$  for the wall fluid ( $r_i \leq r \leq R$ ),  $\rho_l$  and  $\mu_l$  are respectively the density and the viscosity of the two fluids. The continuity equation for incompressible fluids is

$$\frac{\partial v_r}{\partial r} + \frac{v_r}{r} + \frac{\partial v_x}{\partial x} = 0. \quad (2.3)$$

On the solid boundary,  $r = R$ , the velocity is zero,  $v(R) = 0$  and  $v$  is finite on the axis ( $r = 0$ ).

At the interface between the two fluids,  $r = r_i$ , the velocity is continuous:

$$[[v]] = 0, \quad (2.4)$$

where the jump in the quantity  $(.)$  across the interface,  $r_i$ , is noted  $[[.]] = (.)_1 - (.)_2$ . The components of the stress tensor  $\boldsymbol{\sigma}$  of a viscous fluid (Guyon *et al.* 2001) are

$\sigma_{ij} = -p\delta_{ij} + \mu(\partial_i v_j + \partial_j v_i)$  where  $i, j$  are either  $x$  or  $r$  and  $\partial_i \equiv \partial/\partial_i$ . The shear stress is continuous at the interface:

$$[[(\boldsymbol{\sigma}\mathbf{n})\mathbf{t}]] = 0, \tag{2.5}$$

where  $\mathbf{n}$  is normal to the interface from liquid 1 to liquid 2,  $\mathbf{t}$  is the tangent vector. Due to surface tension, the normal stress is discontinuous at the interface with:

$$[[(\boldsymbol{\sigma}\mathbf{n})\mathbf{n}]] = 2\kappa\gamma, \tag{2.6}$$

where  $\gamma$  is the surface tension coefficient and  $2\kappa$  is the sum of the two principal curvatures.

In the base flow the core fluid and the wall fluid flow concentrically and co-currently with a straight interface separating them at a distance from the axis  $r = r_i = R_s$  sketched in figure 1. The base flow is stationary and unidirectional along the direction of the cylinder axis  $U(v_x, 0)$ . As  $v_r = 0$ , equation (2.3) leads to  $v_x(r) = U(r)$  and (2.2) to  $P(x)$ . From (2.1), the pressure gradient is constant. The above conditions  $U(0)$  finite,  $U(R) = 0$ , the interface conditions,  $[[U(R_s)]] = 0$ , the continuity of the shear stress,  $[[\mu\partial_r U(r)]] = 0$  and the normal stress jump  $[[[-P]]] = \gamma/R_s$ , lead to the velocity profile (Selvam *et al.* 2007):

$$\left. \begin{aligned} \frac{U_1(r)}{\bar{U}} &= \frac{2(1 + h^2(M - 1) - M(r/R)^2)}{1 + h^4(M - 1)}, & 0 \leq r \leq R_s, \\ \frac{U_2(r)}{\bar{U}} &= \frac{2(1 - (r/R)^2)}{1 + h^4(M - 1)}, & R_s \leq r \leq R, \end{aligned} \right\} \tag{2.7}$$

where  $M = \mu_2/\mu_1$  is the viscosity ratio and  $h = R_s/R$ ;  $\bar{U}$  is the average velocity of the flow. An example of such a velocity profile is given in figure 1.

### 3. Linear stability analysis (LSA)

To study the stability of the core–annular flow, we perturb the base flow and the interface with the axisymmetric disturbances (Sextl 1927),

$$v_x = U(r) + \delta v_x(x, r, t), \quad v_r = \delta v_r(x, r, t), \quad p = P + \delta p, \quad (x, r, t), \quad r_i = R_s + \epsilon(x, r, t), \tag{3.1a-d}$$

where the perturbations are assumed small (first order) compared to the base flow leading to the linearized equations:

$$\rho_l \left( \frac{\partial \delta v_x}{\partial t} + \delta v_r \frac{dU(r)}{dr} + U(r) \frac{\partial \delta v_x}{\partial x} \right) = -\frac{\partial \delta p}{\partial x} + \mu_l \left[ \frac{\partial^2 \delta v_x}{\partial r^2} + \frac{1}{r} \frac{\partial \delta v_x}{\partial r} + \frac{\partial^2 \delta v_x}{\partial x^2} \right], \tag{3.2}$$

$$\rho_l \left( \frac{\partial \delta v_r}{\partial t} + U(r) \frac{\partial \delta v_r}{\partial x} \right) = -\frac{\partial \delta p}{\partial r} + \mu_l \left[ \frac{\partial^2 \delta v_r}{\partial r^2} + \frac{1}{r} \frac{\partial \delta v_r}{\partial r} - \frac{\delta v_r}{r^2} + \frac{\partial^2 \delta v_r}{\partial x^2} \right]. \tag{3.3}$$

The continuity equation, equation (2.3) leads to

$$\frac{\partial \delta v_r}{\partial r} + \frac{\delta v_r}{r} + \frac{\partial \delta v_x}{\partial x} = 0. \tag{3.4}$$

The velocity perturbation should be finite on the axis and zero on the solid boundary of the cylinder,  $\delta v_x(R) = \delta v_r(R) = 0$ . At the perturbed interface,  $r_i = R_s + \epsilon(x, t)$ , the

linearized ( $\sqrt{1 + (\partial_x \epsilon)^2} \simeq 1$ ) normal and tangent vectors are,  $\mathbf{n}(-\partial_x \epsilon, 1)$  and  $\mathbf{t}(1, \partial_x \epsilon)$ . Therefore, the continuity of the velocity at  $r = r_i$ , equation (2.4) leads, for its radial components, to:

$$[[\delta v_r(r_i)]] = [[\delta v_r(R_s)]] = 0. \quad (3.5)$$

For its axial component, one needs to take into account that we have at order one:  $U(r_i) = U(R_s) + (dU(r))/dr\epsilon$ . Remembering that  $[[U(R_s)]] = 0$  for the base flow, leads to:

$$[[U(r_i) + \delta v_x(r_i)]] = \left[ \left[ \frac{dU(r)}{dr}\epsilon + \delta v_x(R_s) \right] \right] = 0. \quad (3.6)$$

As already noticed in Joseph & Renardy (1992a,b), it is important to stress that this equation implies that  $\delta v_x$  is not continuous across the interface at  $r_i$ . Indeed, it is this jump in the shear rate that destabilizes the flow (Hinch 1984). Note that, in the Kelvin–Helmholtz interfacial instability (Kelvin 1870; Helmholtz 1890), this is the jump in velocity, and not of its derivative, which is responsible for the instability.

After linearization and taking into account the relationships,  $[[\mu U'(R_s)]] = 0$  and  $[[\mu U''(R_s)]] = 0$ , the continuity of the shear stress (2.5) leads to:

$$\left[ \left[ \mu \left( \frac{\partial \delta v_x}{\partial r} + \frac{\partial \delta v_r}{\partial x} \right) \right] \right] = 0. \quad (3.7)$$

The linearization of the sum of the two principal curvatures for the deformed interface is  $2\kappa = \partial_{xx}\epsilon - 1/(R_s + \epsilon) \simeq \partial_{xx}\epsilon - 1/R_s + \epsilon/R_s^2$ . Using the base flow relation,  $[[ -P]] = \gamma/R_s$ , the linearized normal stress jump (2.6) is:

$$\left[ \left[ -\delta p + 2\mu \frac{\partial \delta v_r}{\partial r} \right] \right] = \gamma \left( \partial_{xx}\epsilon + \frac{\epsilon}{R_s^2} \right). \quad (3.8)$$

Moreover, from the so-called kinematic condition, the normal velocity of both fluids must be equal to the normal velocity of the interface:  $\mathbf{v}_1 \cdot \mathbf{n} = \mathbf{v}_2 \cdot \mathbf{n} = \partial r_i / \partial t$ , which, once linearized, becomes

$$(-\partial_x \epsilon)U(R_s) + \delta v_r(R_s) = \partial_t \epsilon, \quad (3.9)$$

since  $U_1(R_s) = U_2(R_s)$  and  $\delta v_{r,1}(R_s) = \delta v_{r,2}(R_s)$  from (3.5).

#### 4. Normal modes

The axisymmetry of both the base flow and its disturbances and the incompressibility of the fluid (3.4) allows us to use a Stokes streamfunction  $\psi(x, r)$ , for the velocity perturbation:

$$\delta v_x = \frac{1}{r} \frac{\partial \psi}{\partial r} \quad \text{and} \quad \delta v_r = -\frac{1}{r} \frac{\partial \psi}{\partial x}. \quad (4.1a,b)$$

Eliminating the pressure between (3.2) and (3.3) and taking into account (4.1) leads to (Sextl 1927):

$$\left[ \frac{\partial}{\partial t} + U(r) \frac{\partial}{\partial x} \right] D\psi(x, r) - LU(r) \frac{\partial \psi(x, r)}{\partial x} = \frac{1}{Re} DD\psi(x, r), \quad (4.2)$$

where we have defined the operators  $D = \partial^2 / \partial r^2 - (1/r)(\partial / \partial r) + (\partial^2 / \partial x^2)$  and  $L = (d^2 / dr^2) - (1/r)(d/dr) = r(d/dr)((1/r)(d/dr))$ . We have normalized lengths by  $R$ ,

velocities by  $\bar{U}$ , time by  $R/\bar{U}$  and pressures by  $\rho\bar{U}^2$ . Hence the normalized interface is localized at  $h = R_s/R$  and the Reynolds number is  $Re = \rho\bar{U}R/\mu$ .

In the linear stability analysis, the perturbations of the interface, streamfunction and pressure are analysed in term of the normal modes of wavenumber  $k$ , frequency  $\omega = ck$  and phase velocity,  $c$ :  $r_i = h + \epsilon_0 e^{ik(x-ct)}$ ,  $\psi = \phi(r)e^{ik(x-ct)}$  and  $\delta p = p e^{ik(x-ct)}$ . Using these time and space dependencies in (4.2), one gets the Orr–Sommerfeld equation for axisymmetric flows (Sexl 1927; Pekeris 1948; Drazin & Reid 1981):

$$(L - k^2)^2 \phi(r) = ikRe\{(U(r) - c)(L - k^2)\phi(r) - (LU(r))\phi(r)\}. \quad (4.3)$$

For a parabolic Poiseuille-like base flow (2.7),  $LU(r) = 0$  and the last term of (4.3) vanishes. In this latter case, Sexl (1927), Pekeris (1948), Drazin & Reid (1981) have shown that the Orr–Sommerfeld equation can be integrated to give:

$$(L - k^2)\phi(r) = f(r), \quad (4.4)$$

where

$$(L - k^2)f(r) = ikRe(U(r) - c)f(r). \quad (4.5)$$

This problem is thus reducible to an inhomogeneous second-order equation. Equation (4.3) governs the behaviour of each fluid with Stokes streamfunctions  $\psi_1$  and  $\psi_2$  for the core and wall fluid, respectively. For the wall fluid, the rigid boundary conditions at the wall are written  $\phi_2(1) = \phi_2'(1) = 0$ . At the interface between the two fluids ( $r_i = h + \epsilon$ ), we rewrite the five above equations (3.5), (3.6), (3.7), (3.8) and (3.9) in a dimensionless form using (4.1) and the  $e^{ik(x-ct)}$  dependence of  $\epsilon$  and  $\psi$ .

The kinematic conditions (3.9) and (3.5) lead to

$$\phi_1(h) = \phi_2(h) = -h(U(h) - c)\epsilon_0, \quad (4.6)$$

where

$$U(h) = U_1(h) = U_2(h) = \frac{2(1 - h^2)}{1 + h^4(M - 1)} \quad (4.7)$$

is the dimensionless velocity of the base flow at the interface (2.7) and we define  $\phi(h) = \phi_1(h) = \phi_2(h)$ .

The continuity of the axial component of the velocity, equation (3.6), is written as:

$$[U_1'(h) - U_2'(h)]h\epsilon_0 + [\phi_1'(h) - \phi_2'(h)] = 0. \quad (4.8)$$

Note that  $\epsilon_0$  can be eliminated in the latter using (4.6). The continuity of the shear stress, equation (3.7), is written as

$$h\phi_1''(h) - \phi_1'(h) + k^2 h\phi(h) = M[h\phi_2''(h) - \phi_2'(h) + k^2 h\phi(h)]. \quad (4.9)$$

For the jump of the normal stress (3.8), extracting the pressure  $\delta p_l$  from (3.2), using the kinematic condition (4.6) and keeping only the linear terms, we get

$$\begin{aligned} & [[\eta(h^2\phi'''(h) - h\phi''(h) + (1 - 3k^2h^2)\phi'(h) + 2k^2h\phi(h)) \\ & + ikh^2Re\{\zeta((c - U(h))\phi'(h) + U'(h)\phi(h))\}]] + \frac{ik(1 - k^2h^2)\phi(h)}{(c - U(h))Ca} = 0, \end{aligned} \quad (4.10)$$

where  $\eta_1 = \zeta_1 = 1$ ,  $\eta_2 = M$  and  $\zeta_2 = \zeta = \rho_2/\rho_1$  is the density ratio of the two fluids and  $Re = \rho_1\bar{U}R/\mu_1$  is the reference Reynolds number.  $Ca = \mu_1\bar{U}/\gamma$  is the dimensionless capillary number which compares viscous forces to surface tension ones ( $\gamma$ ).

Before addressing the general case of two immiscible fluids at any  $Re$  number, let us focus on the creeping flow limit ( $Re \rightarrow 0$ ).

5. Immiscible case in the creeping flow limit ( $1/Ca \neq 0, Re = 0$ )

As discussed above, the dispersion relation for immiscible fluids has been investigated in the literature in several studies. We note however that Herrada *et al.* (2008) did not use the correct expressions (3.6) and (4.8) for the continuity of the axial component of the velocity at the interface. In their work Guillot *et al.* (2007, 2008) used the correct boundary conditions but their approach is based on the perturbation of the lubrication equation, assuming hence a long wave approximation. To compare with these different approaches we compute now the complete solution. In the creeping flow limit ( $Re = 0$ ), the Orr–Sommerfeld equation (4.3) reduces to:

$$(L - k^2)^2 \phi = 0, \tag{5.1}$$

the solution of which is a linear combination of Bessel functions (Abramowitz & Stegun 1964),  $rI_1(kr)$ ,  $rK_1(kr)$ ,  $r^2I_0(kr)$  and  $r^2K_0(kr)$ . (The Bessel functions  $I_n(z)$  and  $K_n(z)$  are solutions of the differential equation  $z^2 d^2w/dz^2 + z dw/dz - (z^2 + n^2)w = 0$ .) For the core fluid, the regularity of the velocity at the  $r = 0$ , implies

$$\phi_1 = A_1 rI_1(kr) + C_1 r^2 I_0(kr) \tag{5.2}$$

and for the wall fluid, we have:

$$\phi_2 = A_2 rI_1(kr) + B_2 rK_1(kr) + C_2 r^2 I_0(kr) + D_2 r^2 K_0(kr), \tag{5.3}$$

where the solid boundary condition, zero velocity at the wall ( $r = 1, \phi_2(1) = \phi_2'(1) = 0$ ) leads to two equations relating  $A_2, B_2, C_2$  and  $D_2$ . Using these two equations and the four interfacial conditions (4.6), (4.8), (4.9) and (4.10) (with  $Re = 0$ ), we obtain the dispersion relation from the compatibility conditions of these six equations as the zero of the  $6 \times 6$  determinant:

$$0 = \begin{vmatrix} I_1(kh) & I_0(kh) & I_1(kh) & K_1(kh) & I_0(kh) & K_0(kh) \\ khI_1' - \frac{\beta}{\Delta} I_1 & (I_0 + khI_0') - \frac{\beta}{\Delta} I_0 & khI_1' & khK_1' & (I_0 + khI_0') & (K_0 + khK_0') \\ khI_1 & khI_0 + I_0' & MkhI_1 & MkhK_1 & M(khI_0 + I_0') & M(khK_0 + K_0') \\ 2k^2 h^2 I_1' - \frac{i\Gamma}{\Delta} I_1 & 2k^2 h^2 I_0' - \frac{i\Gamma}{\Delta} I_0 & 2Mk^2 h^2 I_1' & 2Mk^2 h^2 K_1' & 2Mk^2 h^2 I_0' & 2Mk^2 h^2 K_0' \\ 0 & 0 & hI_1(k) & hK_1(k) & I_0(k) & K_0(k) \\ 0 & 0 & khI_1'(k) & khK_1'(k) & I_0(k) + kI_0'(k) & K_0(k) + kK_0'(k) \end{vmatrix} \tag{5.4}$$

where

$$\Delta = c - U(h), \quad \beta = h(U_2'(h) - U_1'(h)) = \frac{4h^2(M - 1)}{(1 + h^4(M - 1))}, \quad \Gamma = \frac{(1 - k^2 h^2)}{Ca}. \tag{5.5a-c}$$

The interfacial velocity,  $U(h)$  is given in (4.7). When not mentioned, the variable of any  $I_n$  is  $kh$  ( $I_n = I_n(kh), I_n' = I_n'(kh)$ , etc.). It should be noticed that the above determinant is a polynomial of second degree in terms of  $\Delta$ . Moreover, by considering the second and fourth lines, it appears that  $\Delta = 0$  is a root of the polynomial. (Multiplying the second and fourth lines by  $\Delta$  and then making  $\Delta = 0$  leads to a determinant with two proportional lines; hence the determinant is equal to 0.) This leaves only one non-trivial root. Noting that the only term involving  $Ca, i\Gamma/\Delta$ , is imaginary, the solution can be written in a compact form:

$$c = U(h) - \beta s(M, h, k) + \frac{i(1 - k^2 h^2)}{Ca} q(M, h, k), \tag{5.6}$$

where  $s(M, h, k)$  and  $q(M, h, k)$  are real when  $k$  is real.

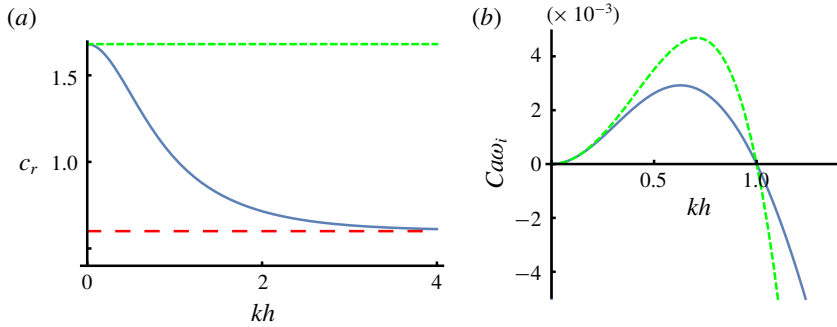


FIGURE 2. (Colour online) Creeping flow,  $Re = 0$ . (a) Phase velocity,  $c_r$ , versus the dimensionless wave vector  $kh$ . (b) Product  $Ca\omega_i$  of the capillary number and the growth rate versus the dimensionless wave vector  $kh$ .  $M = 25$  and  $h = 0.5$ . In both figures, the full blue curves correspond to the phase velocity and growth rate from the creeping flow dispersion equation, equation (5.6). The green short dotted lines correspond to the same items from Guillot *et al.* (2007, 2008). In (a) the top horizontal short dotted green line is the long wave phase velocity,  $\tilde{V}_{LW}$ , the horizontal large dashed red line at the bottom corresponds to the short wave phase velocity.

In figure 2, we have plotted the phase velocity,  $c_r = \text{Re}(c)$ , as a function of the wavenumber  $kh$ . As expected, the phase velocity varies smoothly from its long wave limit,

$$\tilde{V}_{LW} = \frac{2(1-h^2)(1+(M-1)h^2)}{(1+(M-1)h^4)^2}, \quad (5.7)$$

to its short wave one, which is the interface velocity  $U(h)$ . This is a classical result (Charru & Fabre 1994) for a temporal instability ( $k$  real). The zero-order phase velocity,  $\tilde{V}_{LW}$ , can be obtained by differentiating the relative flux with respect of  $h$ ,  $\tilde{V}_{LW} = \partial(hU_1(h))/\partial h$  (Charru & Fabre 1994; Lajeunesse *et al.* 1999). Note that, when  $M = 1$ ,  $\beta = 0$  and the second term vanishes: the phase velocity is constant.

The temporal growth rate of the instability is related to the imaginary part of the dispersion relation,  $\omega_i = \text{Im}(ck) = c_i k$ , and is given by the last term of (5.6). It is inversely proportional to the capillary number. Moreover, we have checked that, for arbitrary values of  $M$ ,  $h$  and  $k$ ,  $q(M, h, k)$  is positive. Therefore, the stability is determined by the sign of  $(1 - k^2 h^2)$ . More specifically, the interface is unstable for long waves and stable for small ones. This is physically intuitive as shorter wavelength increases the area between the two fluids and hence its surface energy promoting stability like for the Rayleigh–Plateau instability of a static liquid column (Rayleigh 1899). In figure 2(b), the plot of the product  $Ca\omega_i$  of the capillary number and the growth rate versus the dimensionless wavenumber  $kh$  for a given viscosity ratio ( $M = 25$ ) shows the change from instability to stability at  $kh = 1$ .

### 5.1. Comparison with results from the literature

We compare these results with those of the literature. In Herrada *et al.* (2008), the approach is very similar to ours, with same (5.2) and (5.3), but the authors assume that the longitudinal velocity perturbation,  $\delta v_x$ , is continuous at the interface, in contradiction to (3.6) and (4.8) and with Joseph & Renardy (1992a,b). This assumption leads to  $\phi'_1(h) = \phi'_2(h)$ , which, using (4.8), is formally equivalent to putting

$\beta = 0$  in our creeping flow determinant, leading to  $c = U(h) + i(1 - k^2 h^2)q(M, h, k)/Ca$ . The only difference with (5.6) is the phase velocity which becomes independent of the wave vector and equal to  $U(h)$ , the interfacial velocity of the base flow. In Guillot *et al.* (2007, 2008), the boundary conditions are the same as ours, but the use of a lubrication approximation, i.e. a development at long wavelengths, leads to an oversimplified dispersion relationship that is written in our notations:  $c = \tilde{V}_{LW} + ikh(1 - k^2 h^2)f(M, h)/Ca$ . Compared to the development at long wavelengths of (5.6):  $c = \tilde{V}_{LW} + c_2(M, h)k^2 h^2 + ikhf(M, h)(1 - g(M, h)k^2 h^2)/Ca + \dots$ , the frequency dispersion is neglected. In figure 2, the short green dotted lines correspond to Guillot *et al.* (2007, 2008). As expected, the two curves are in agreement in the long wave limit.

### 5.2. Convective–absolute transition for creeping flows

We refer the reader to the chapter of Huerre and Rossi in Godreche & Manneville (1998) and to Huerre & Monkewitz (1990) for an introduction to the basic concepts of convective and absolute instabilities. Here, we briefly describe the numerical procedure to identify the transition from convective to absolute instability. When an unstable open flow is locally perturbed by a small disturbance, the growing wave packet can display two different types of evolution (Briggs 1964; Godreche & Manneville 1998). For a convectively unstable flow (CU), the disturbances are amplified and advected away from their initial location. Such a convectively unstable flow behaves like a noise amplifier. For an absolutely unstable flow (AU), although advected, the wave packet is so strongly amplified that it invades the whole space (downstream and upstream).

In a temporal stability framework, the perturbations are assumed to be periodic in the axial direction, i.e. for a given real wavenumber  $k = k_r$ , we seek a complex frequency  $\omega = \omega_r + i\omega_i$ . In the spatial stability framework, the perturbations are time periodic, i.e. for a given real frequency  $\omega = \omega_r$ , we seek a complex spatial wavenumber  $k = k_r + ik_i$ . In a spatio-temporal setting (as required for determining the absolute/convective nature of the instability), both the frequency and wavenumber may be complex. In the case of an absolutely unstable flow, one frequency mode will prevail at long times and the system will behave like a self-sustained resonator (see Godreche & Manneville (1998) for more details). The transition from a convective instability to an absolute one can be determined from the dispersion relation (Huerre & Monkewitz 1990) considering complex wavenumbers  $k = k_r + ik_i$  as well as complex frequencies  $\omega = \omega_r + i\omega_i$ . For instance, the transition corresponds to the pinching of two spatial branches of the dispersion equation. Therefore, the transition can be determined directly, in our problem, from the dispersion relation. This is readily done using the following procedure of Godreche & Manneville (1998): the transition between a convective instability and an absolute one corresponds to a complex critical wavenumber  $k_c$  and frequency  $\omega_c$  for which the group velocity  $v_g(k) = \partial\omega/\partial k$  and the temporal growth rate  $\omega_i$  are both zero, namely:

$$v_g(k_c) = \left. \frac{\partial\omega}{\partial k} \right|_{k=k_c} = 0 \quad \text{and} \quad \omega_i(k_c) = 0. \tag{5.8a,b}$$

Using the above dispersion equation (5.6), we can analyse the convective–absolute transition. For a given  $h$  and a given  $M$ , the complex frequency is a function of  $k$  and  $Ca$ :  $\omega(k, Ca) = c(k, Ca)k$ . For a range of values of  $Ca$ , we compute the wave vectors  $k_0(Ca)$  which have a zero group velocity  $v_g(k_0(Ca)) = 0$ . We then compute  $\omega(k_0(Ca))$ .

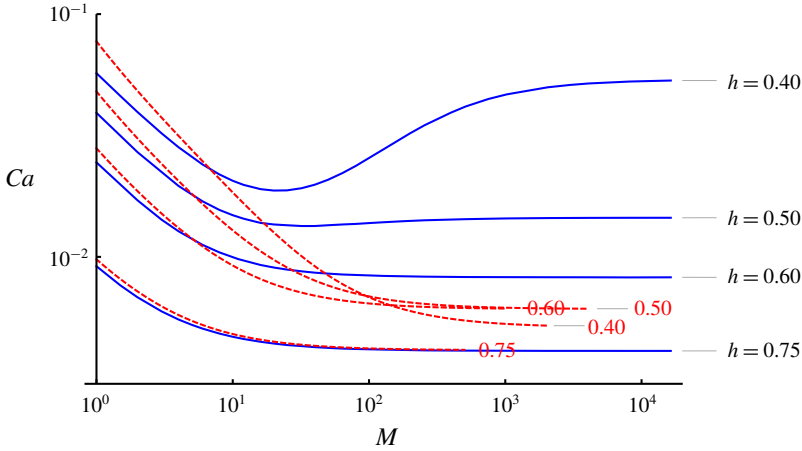


FIGURE 3. (Colour online) The transition from convective instability to absolute instability in a log–log plot of the capillary number,  $Ca$ , versus the viscosity ratio,  $M$ . The instability is absolute below the curve associated with the corresponding interface location  $h$  and convective above. The full blue curves correspond to our full calculation using (5.6) and (5.8), with the corresponding  $h$  given on the right of the figure. The red monotonic dashed lines correspond to the approximated solution of Guillot *et al.* (2007, 2008), with the corresponding value of  $h$  on each curve (0.4, 0.5, 0.6, 0.75).

The transition between a convective instability and an absolute one corresponds to  $Ca^*$  such that  $\omega_i(k_0(Ca^*)) = 0$ . For  $k_c = k_0(Ca^*)$ , equation (5.8) is then fulfilled. (When there are multiple roots for  $k_c$ , we choose the one for which the plot  $\omega_i(\omega_r)$  pinches at  $\omega_i = 0$ . As  $Ca$  is changed, we follow this root through continuity.)

In figure 3, we plot a series of convective–absolute transition curves,  $Ca$  versus  $M$  for different  $h$  values (full blue lines). The instability is absolute below the curves and convective above. Moreover, for large value of  $h \geq 0.45$ , the curves are monotonic, meaning that on increasing  $M$  at constant  $Ca$ , there is only a transition from absolute to convective instabilities. For smaller values the curves exhibit a minimum, meaning that the instability is absolute below a certain viscosity ratio  $M_{min}$  and above another one  $M_{max}$  whereas it is convective in the range  $M_{min} < M < M_{max}$ . The dashed lines correspond to the results of Guillot *et al.* (2007, 2008) where the dispersion term was discarded, as discussed above. We note that unlike our results, variations obtained by these authors are all monotonic. For  $h = 0.75$  the two sets of curves are very close. The discrepancy is significant for smaller values of  $h$  and especially for large  $M$  values where it can reach one order of magnitude.

## 6. General case ( $1/Ca \neq 0$ , $Re \neq 0$ )

Now, we seek to extend this analysis to the more general case of the two immiscible fluids of different viscosity, density and inertia. In order to get  $\phi_1(r)$  and  $\phi_2(r)$ , we have to solve the Orr–Sommerfeld equations (4.4) and (4.5). The solution of the homogenous part of (4.4), with  $f = 0$ , is a combination of Bessel functions of the first kind,  $I_1(kr)$  and  $K_1(kr)$ . Moreover, the solutions  $f$  of (4.5), for a parabolic Poiseuille flow in a circular pipe ( $U(r) \equiv A + Br^2$ ), can be expressed in terms of confluent hypergeometric functions, i.e. Kummer functions (Pekeris 1948; Drazin & Reid 1981). (Kummer functions,  $M(a, 2, z)$  and  $U(a, 2, z)$  are solutions of the confluent

hypergeometric differential equation:  $z^2 w''/dz^2 + (2 - z) dw/dz - aw = 0$  (Abramowitz & Stegun 1964). Equation (4.5) becomes identical to this latter differential equation after simple variable changes such as  $f(r) = z \exp(-z/2)M(a, 2, z)$  and  $z = br^2$  (Pekeris 1948).) Using these solutions,  $f(r)$  of (4.5), we integrate the full equation (4.4) to obtain the streamfunction for each fluid expressed in term of Bessel functions of the first kind and Kummer functions. Each solution requires us to fulfil the appropriate boundary condition, namely a zero velocity at  $r = 1$  for the wall fluid and the regularity at  $r = 0$  for the core fluid velocity.

For the core fluid ( $U(r) = U_1(r)$ ) the solution which is regular at the origin,  $r = 0$  Pekeris (1948) is:

$$\left. \begin{aligned} \phi_1(r) &= A_1 r I_1(kr) + B_1 r \int_0^r (I_1(kr)K_1(kt) - I_1(kt)K_1(kr))m_1(t) dt \\ &\quad \text{with } m_1(r) = r^2 e^{-b_1 r^2/2} M(a_1, 2, b_1 r^2), \\ b_1 &= \sqrt{kRe_1} e^{3i\pi/4}, \quad a_1 = 1 - \frac{b_1}{4} \left( 1 - c \frac{1 + (M-1)h^4}{2M} - \frac{M-1}{M} (1-h^2) \right) + \frac{k^2}{4b_1}. \end{aligned} \right\} \tag{6.1}$$

$Re_1 = Re(2M)/(1 + (M-1)h^4)$  is a modified Reynolds number ( $Re = \rho_1 \bar{U}R/\mu_1$ ).

Taking into account the boundary conditions at  $r = 1$  ( $\delta v_2(1) = \mathbf{0}$ ,  $\phi_2(1) = \phi_2'(1) = 0$ ), the solution for the wall fluid ( $U(r) = U_2(r)$ ) is:

$$\left. \begin{aligned} \phi_2(r) &= A_2 r \int_r^1 (I_1(kr)K_1(kt) - I_1(kt)K_1(kr))u_2(t) dt \\ &\quad + B_2 r \int_r^1 (I_1(kr)K_1(kt) - I_1(kt)K_1(kr))m_2(t) dt, \\ &\quad \text{with } u_2(r) = b_2 r^2 e^{-b_2 r^2/2} U(a_2, 2, b_2 r^2), \quad m_2(r) = r^2 e^{-b_2 r^2/2} M(a_2, 2, b_2 r^2), \\ Re_2 &= Re_1/M^2, \quad b_2 = \sqrt{kRe_2} e^{3i\pi/4}, \quad a_2 = 1 - \frac{b_2}{4} \left( 1 - c \frac{1 + (M-1)h^4}{2} \right) + \frac{k^2}{4b_2}. \end{aligned} \right\} \tag{6.2}$$

We note that, due to the form of the Orr–Sommerfeld equation (4.3), the wavenumber  $k$  is involved both alone and through the combination  $kRe$  which in the present case of confluent hypergeometric function appears as  $\sqrt{kRe}$ . With these two streamfunctions, we are left with four unknown constants ( $A_1, B_1, A_2, B_2$ ) which will be determined together with  $\epsilon_0$  by the physical conditions at the interface between the two fluids located at  $r_i = h + \epsilon_0 e^{ik(x-ct)}$ .

They are linked by the four equations (4.6), (4.8), (4.9) and (4.10). For a non-trivial solution of this system of equations, the  $4 \times 4$  determinant corresponding to the compatibility of these four unknowns must be equal to zero, leading to the dispersion relation given by the complex phase velocity function  $c(M, \zeta, h, k, Re, Ca)$ .

After tedious calculations, but with numerous simplifications due to the many properties of Bessel and Kummer functions (Abramowitz & Stegun 1964), the bulk equations (6.1) and (6.2) and the interface conditions lead to the  $4 \times 4$  determinant corresponding to:

$$0 = \begin{vmatrix} I_1(kh) & p_1 & p_{21} & p_{22} \\ \Delta kh I_1'(kh) - \beta I_1(kh) & \Delta kh q_1 - \beta p_1 & \Delta kh q_{21} & \Delta kh q_{22} \\ 2(M-1)k^2 h^2 I_1(kh) & 2(M-1)k^2 h^2 p_1 - hm_1(h) & Mhu_2(h) & Mhm_2(h) \\ 2k^3 h^3 I_1'(kh) - i\gamma_1 & 2k^3 h^3 q_1 - h^2 m_1'(h) - i\pi_1 & M(2k^3 h^3 q_{21} + h^2 u_2'(h)) & M(2k^3 h^3 q_{22} + h^2 m_2'(h)) \end{vmatrix} \tag{6.3}$$

with

$$\gamma_1 = \frac{kh(1 - k^2h^2)I_1(kh)}{\Delta Ca} + kh^2 Re(\zeta - 1)[\Delta(I_1(kh) + khI_1'(kh)) + hU_1'(h)I_1(kh)], \quad (6.4)$$

$$\pi_1 = \frac{kh(1 - k^2h^2)p_1}{\Delta Ca} + kh^2 Re(\zeta - 1)[\Delta khq_1 + hU_1'(h)p_1] \quad (6.5)$$

and  $\Delta$ ,  $U(h)$  and  $\beta$  given above in (5.5).

The determinant is written in order to avoid divergence at  $k = 0$  and using only a Bessel function of the first kind and its first derivatives ( $I_1, I_1', K_1, K_1'$ ). The many different other terms involve Bessel and confluent hypergeometric functions, namely:

$$\left. \begin{aligned} p_1(k, h) &= I_1(kh) \int_0^h K_1(kt)m_1(t) dt - K_1(kh) \int_0^h I_1(kt)m_1(t) dt, \\ q_1(k, h) &= I_1'(kh) \int_0^h K_1(kt)m_1(t) dt - K_1'(kh) \int_0^h I_1(kt)m_1(t) dt, \\ p_{21}(k, h) &= I_1(kh) \int_h^1 K_1(kt)u_2(t) dt - K_1(kh) \int_h^1 I_1(kt)u_2(t) dt, \\ q_{21}(k, h) &= I_1'(kh) \int_h^1 K_1(kt)u_2(t) dt - K_1'(kh) \int_h^1 I_1(kt)u_2(t) dt, \\ p_{22}(k, h) &= I_1(kh) \int_h^1 K_1(kt)m_2(t) dt - K_1(kh) \int_h^1 I_1(kt)m_2(t) dt, \\ q_{22}(k, h) &= I_1'(kh) \int_h^1 K_1(kt)m_2(t) dt - K_1'(kh) \int_h^1 I_1(kt)m_2(t) dt. \end{aligned} \right\} \quad (6.6)$$

In the determinant, we can identify different contributions. The effect of the capillarity is present in the two terms,  $\gamma_1$  and  $p_1$ , involving  $\Gamma = (1 - k^2)/Ca$  as for the above creeping flow limit (5.5). These two terms account for the Rayleigh–Plateau instability (Rayleigh 1899). The term  $\beta$  characterizes the jump in the shear rate accounting for the pseudo Kelvin–Helmholtz instability mechanism (Kelvin 1870; Helmholtz 1890; Hinch 1984).

Equating the above determinant to zero represents thus an implicit dispersion function which relates  $k$  and  $c$  for a given set of parameters ( $M, \zeta, h, Re, Ca$ ). It is important to note that this dispersion relationship is exact, as it involves no approximations such as a short (or long) wavelength. The equation represents thus the central result of this paper. It is also very general as it takes into account a contrast of density or viscosity and a surface tension. This relationship is however cumbersome to manipulate because of its implicit form and it involves non-trivial functions, although they are present in many software libraries. It should be noted, however, that a numerical problem must be solved all the same. But solving the determinant is quite simple without any particular ‘numerical’ knowledge being required to discretize the linear disturbance equations and solve a problem with eigenvalues as in Selvam *et al.* (2007, 2009).

We have already considered the case of immiscible fluids in the creeping flow regime corresponding to  $Re = 0$ . (The solution of the creeping flow could have been addressed from the general case, but it is a very heavy calculation requiring a considerable amount of asymptotics.) We will now apply our general approach to the case of iso-dense fluids ( $\zeta = 1$ ) with a straight interface between the two fluids

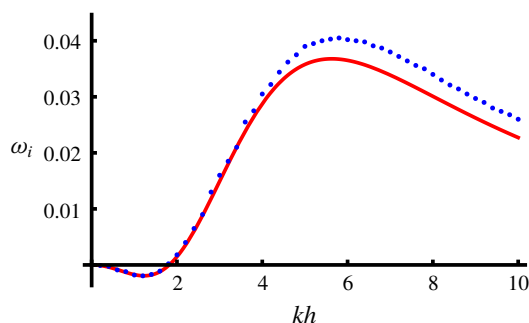


FIGURE 4. (Colour online) Comparison between our full calculation of the growth rate,  $\omega_i$ , versus the dimensionless wave vector  $kh$  (full red line) with the results (blue dots) of Selvam *et al.* (2007) (dashed line in their figure 5a) for  $M = \exp(1)$ ,  $Re = \exp(1)$  and  $h = 0.5$ .

but without significant interfacial tension ( $1/Ca = 0$ ) which leads to  $\gamma_1 = \pi_1 = 0$  in (6.4)–(6.5). This interface may also be understood as the pseudo-interface between two miscible fluids in the absence of diffusion, i.e. at high Schmidt number ( $Sc = \infty$ ). The analogy between these two situations has been already applied to the displacement of one fluid by another one in a capillary tube (Chen & Meiburg 1996; Petitjeans & Maxworthy 1996). We will investigate the stability of this system but also the convective or absolute nature of this instability and compare our results to the literature.

### 7. Matched density without surface tension ( $\zeta = 1$ and $1/Ca = 0$ ).

As discussed above, the determination of the dispersion function requires us to determine the zero of the determinant which relates  $c$  and  $k$  for a given set of parameters,  $(M, h, Re)$ . In this procedure to find numerically the dispersion function, for each value of  $k$ , we scan the real and imaginary parts of  $c$  until reaching a zero value of the determinant (for both its real and imaginary parts). As a benchmark, we compare our full calculation with the numerical study of Selvam *et al.* (2007). In figure 5(a) of their paper, the authors display the temporal growth rate versus the dimensionless wave vector  $kh$  for two miscible fluids in the absence of diffusion ( $Sc = \infty$ ), i.e. a sharp interface without surface tension with the set of parameters  $M = \exp(1)$ ,  $Re = \exp(1)$  and  $h = 0.5$  in our notations. The comparison is shown in figure 4: our results are 5% smaller, but there is not enough detail on the calculations used in Selvam *et al.* (2007) to find the origin of this, although small, difference.

Figure 5 displays a set of variations of the phase velocity,  $c_r$  (a), and of the imaginary part of the velocity,  $c_i = \omega_i/k$  (b) versus the dimensionless real wave vector  $kh$  for  $M = 30$  and  $h = 0.35$  at different Reynolds numbers. It worth noting that in the long wave limit, the mode remain stable for thin enough core fluid  $h = 0.35$  as already noticed by Hickox (1971).

#### 7.1. Long wave expansion

For calculation purposes, it could be useful to have a simpler expression for the dispersion relation. We note again that, due to the form of the Orr–Sommerfeld equation (4.3), the wavenumber  $k$  is involved both alone and through the combination

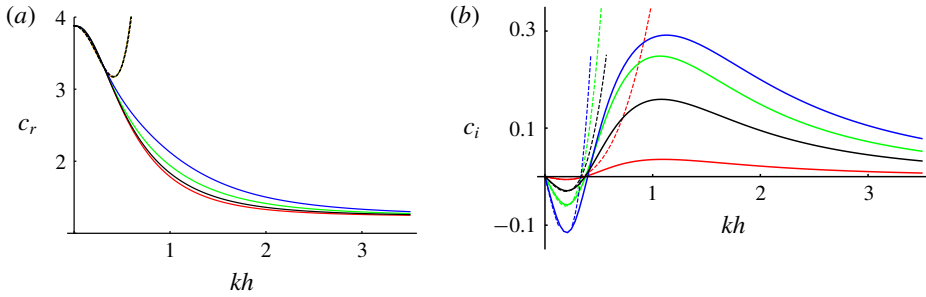


FIGURE 5. (Colour online) Phase velocity,  $c_r$  (a), and imaginary part of the velocity,  $c_i = \omega_i/k$  (b) versus dimensionless wave vector  $kh$  for  $M = 30$  and  $h = 0.35$ . The different continuous lines correspond to different Reynolds numbers: red,  $Re = 1$ ; brown,  $Re = 5$ ; green,  $Re = 10$  and blue,  $Re = 20$ . The dashed lines close to the low  $kh$  parts of the full curves, correspond to the long wave expansion (7.1). The dashed line in (a) corresponds to the phase velocity in the creeping flow limit ( $Re = 0$ ), equation (5.6).

$kRe$  in the different hypergeometric functions. Therefore it is possible to perform a long wave expansion, i.e. series expansion of the Bessel and hypergeometric functions at small values of both  $k$  and  $kRe$ . Using the Mathematica software, we get the following explicit development to order four of the complex velocity:

$$c(M, h, k, Re) = c_{0,0} + ikRe c_{1,1} + k^2(c_{2,0} + c_{2,2}Re^2) + ik^3Re(c_{3,1} + c_{3,3}Re^2) + k^4(c_{4,0} + c_{4,2}Re^2 + c_{4,4}Re^4) + O(k^5). \quad (7.1)$$

The coefficients  $c_{n,m}(M, h)$  are real and depend only of the viscosity ratio  $M$  and of the location of the interface  $h$ . The leading term,  $c_{0,0} = \tilde{V}_{LW}$  (5.7) as expected. We note that, the coefficient of the even powers of  $k$  and  $kRe$  are real whereas the odd ones are imaginary. The  $O(1)$  term appears in the temporal growth rate  $\omega_i = \text{Im}(ck) = Re c_{1,1} k^2 + \dots$  and thus determines the long wave stability of the problem. The  $O(2)$  term appears in the expression of the dispersion of the phase velocity and so on. We note that, the  $O(0)$  and  $O(1)$  results are in agreement with the long wave expansion obtained by Renardy (1987) and Joseph & Renardy (1992b). Figure 6 shows the variation with  $h$  of six of these coefficients for a viscosity ratio  $M = 30$ . The coefficients  $c_{2,0}$  and  $c_{4,0}$  are the same as those obtained above for  $Re = 0$  ( $c_2 = c_{2,0}$ ). We note that the long wave coefficient  $c_{1,1}$  changes sign as function of  $h$  which shows that long wave modes are stable for a thin enough core fluid for  $M > 1$ . It is worth mentioning that the third-order term also becomes positive, which means that the system could be unstable at a lower  $h$  than predicted only by the first order. For a given couple  $(M, h)$ , we obtain the explicit complex velocity to the fourth order and therefore the dispersion relationship to the fifth order ( $\omega = ck$ ). In figure 5 we have plotted the comparison with the full solution. The agreement is quite good, as expected for low values of  $kh$ . However, the discrepancy becomes very significant for  $kh > 1$  even including the fifth-order terms.

## 7.2. Convective–absolute transition

The main characteristics of convective and absolute instability have already been described in the subsection on creeping flow. Absolute instability can be identified

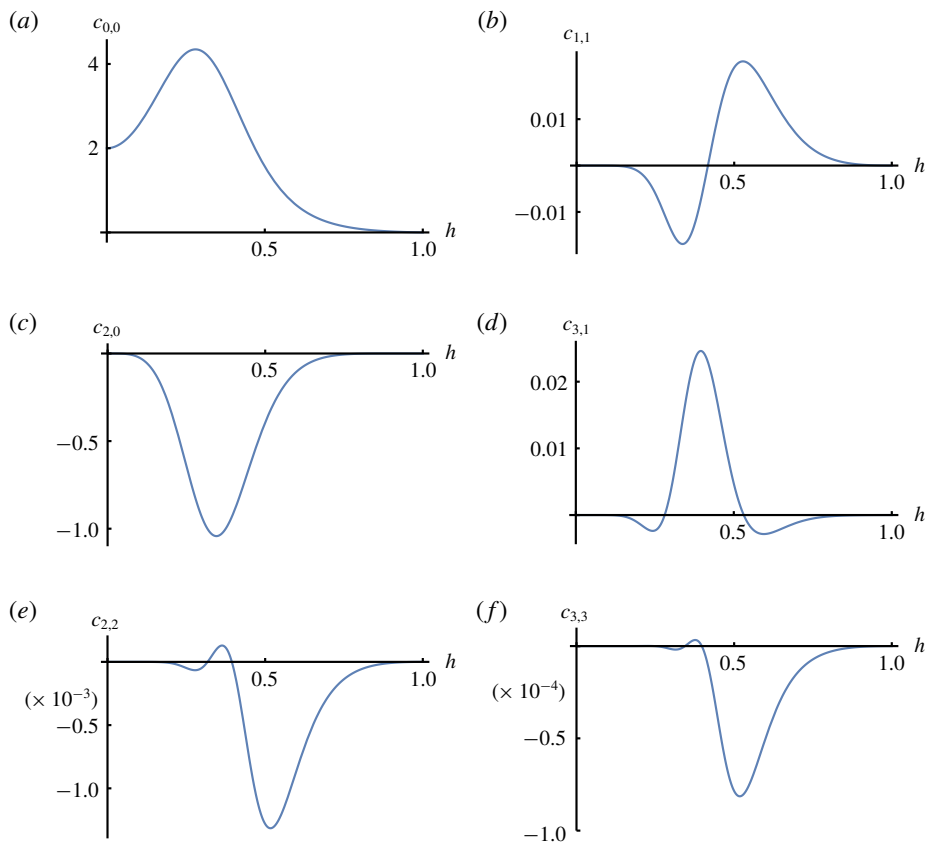


FIGURE 6. (Colour online) Coefficients  $c_{n,m}(M, h)$  of the long wave expansion of the complex instability velocity  $c(M, h, k, Re)$ , equation (7.1), versus  $h$  for  $M = 30$ . First column from top to bottom, coefficients of the real part of  $c$ :  $c_{0,0}$ ,  $c_{2,0}$ ,  $c_{2,2}$ . Second column, coefficients of the imaginary part of  $c$ :  $c_{1,1}$ ,  $c_{3,1}$ ,  $c_{3,3}$ .

numerically by Briggs’ method (Briggs 1964), which presents a mapping procedure involving the identification of the pinching or saddle point of two spatial branches in the complex  $k$  plane. If we define the complex frequency corresponding to the pinching point as  $\omega_0$ , then the flow is absolutely unstable (AU) if the imaginary part  $\omega_0, i$  is positive. Thus,  $\omega_0, i$  represents the absolute growth rate. Although rigorous, the practical problem with Briggs’ method is that it involves mapping the complex plane  $\omega$  to the complex plane  $k$ . If only the pinching point is of interest, iterative algorithms can be used (Deissler 1987). These use the fact that, at the pinching point, the group velocity vanishes ( $vg = \partial\omega/\partial k = 0$ ). By interpolating a complex quadratic function for  $v_g$  with  $k$  as an independent parameter, it is possible to find efficiently the saddle point. Here, we follow the iterative procedure described in Yin *et al.* (2000) to find the absolute growth rate. For four wavenumbers ( $k_j, j = 1 - 4$ ) obtained by an initial estimate, we compute a polynomial interpolation of the variations of the complex frequency  $\omega$ ,

$$\omega(k) = \frac{a}{3}(k - k_4)^3 + \frac{b}{2}(k - k_4)^2 + c(k - k_4) + d, \tag{7.2}$$

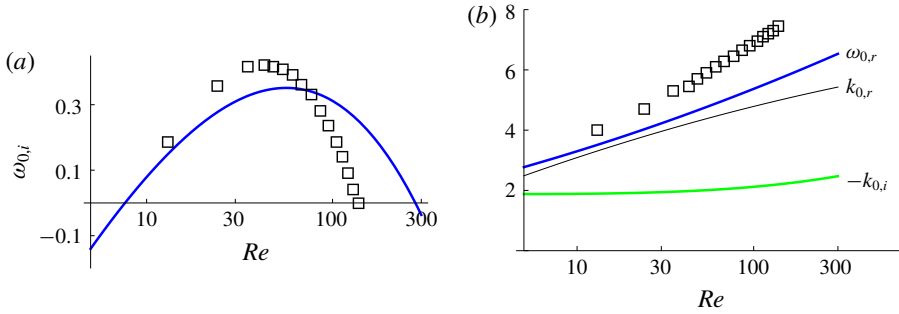


FIGURE 7. (Colour online) Variations of the absolute frequency  $\omega_0$  and absolute wavenumber  $k_0$  versus Reynolds number,  $Re$  for  $M = 25$  and  $h = 0.48$  in a semi-log plot. (a) Imaginary part of the absolute frequency  $\omega_{0,i}$ : positive  $\omega_{0,i}$  corresponds to an absolute instability whereas  $\omega_{0,i} < 0$  corresponds to convective instability; the transition between a convective instability and an absolute one occurs for  $\omega_{0,i} = 0$ . (b) Real part of the absolute frequency,  $\omega_{0,r}$ , real part of the absolute wavenumber,  $k_r$  and opposite of the imaginary part of the absolute wavenumber,  $-k_i$ . The open squares correspond to the values of  $\omega_{0,i}$  (a) and of  $\omega_{0,r}$  (b) from Selvam *et al.* (2009) for a miscible pseudo-interface of thickness  $\delta = 0.008$  and for weak diffusion Schmidt number,  $Sc = \mu/(\rho D_m) = 7500$ .

where  $a, b, c$  and  $d$  are constants to be determined. To do this,  $\omega_j$  is calculated for each of the four  $k_j$  from the above determinant. From the constants found, an improved value for  $k$  is determined using the saddle point criterion  $\partial\omega/\partial k = 0$ ,

$$a(k - k_4)^2 + b(k - k_4) + c. \quad (7.3)$$

Taking the root of this quadratic equation as close as possible to  $k_4$ , a new set of four  $k_j$ s is produced and the above procedure is repeated until convergence is achieved. The corresponding  $\omega$  in the complex plane is the absolute frequency. This algorithm is computationally efficient in the sense that, once the saddle point is found for one parameter, the values of the others can easily be followed through continuation.

Figure 7 displays, on the left, the imaginary part of the absolute frequency  $\omega_{0,i}$  and, on the right, its real part,  $\omega_{0,r}$ , the real part of the absolute wavenumber,  $k_{0,r}$  and the opposite of its imaginary part  $-k_{0,i}$  versus  $Re$  for  $M = 25$  and  $h = 0.48$ . The absolute frequency  $\omega_{0,i}$  is positive over a range of  $Re$  values from  $Re_{min} \simeq 8.0$  to  $Re_{max} \simeq 281$  denoting absolute instability in that range. In figure 8, we plot the same quantities versus  $h$  for  $M = 25$  and  $Re = 48$ . For  $h > 0.40$  and  $h < 0.78$ ,  $\omega_{0,i}$  is positive hence the instability is absolutely unstable in that range.

Our formalism applies to fluids that are inherently immiscible. It is expected that immiscible fluids within the zero surface tension limit will be equivalent to miscible fluids with zero diffusion. Indeed, in both cases, the interface remains sharp and is only subjected to viscous forces. Our results can therefore be qualitatively compared to experiments (d'Olce *et al.* 2009) and simulations (Selvam *et al.* 2009) that studied the absolute convective transition of miscible fluids.

Due to diffusion, the interface between the two fluids is always turbid, leading to a pseudo-interface of thickness  $\delta$ . The numerical analyses have shown (Chen & Meiburg 1996; Kouris & Tsamopoulos 2001, 2002; Kuang *et al.* 2003; Selvam *et al.* 2007, 2009; Talon & Meiburg 2011) that this thickness  $\delta$  also has a strong influence on the stability. One should thus consider the limit of no diffusion and also of a sharp interface, i.e.  $\delta \rightarrow 0$  and  $D_m \rightarrow 0$ .

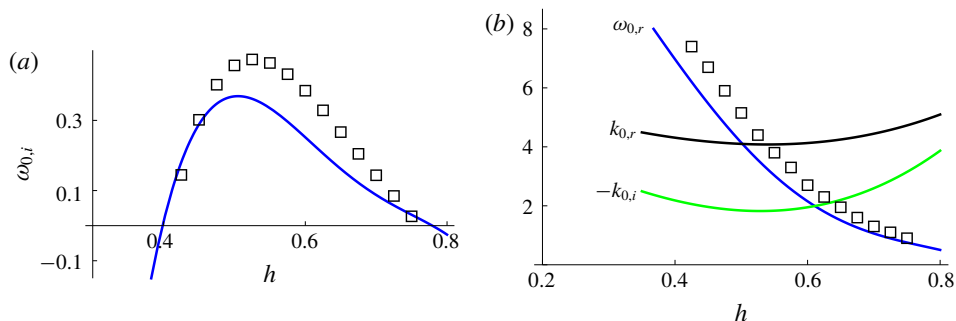


FIGURE 8. (Colour online) Variations of the absolute frequency and absolute wavenumber versus the position of the interface,  $h$  for  $M = 25$  and  $Re = 48$ . (a) Imaginary part of the absolute frequency  $\omega_{0,i}$ . (b) Real part of the absolute frequency,  $\omega_{0,r}$ , real part of the absolute wavenumber,  $k_r$  and opposite of the imaginary part of the absolute wavenumber,  $-k_i$ . The open squares correspond to the values of  $\omega_{0,i}$  (a) and of  $\omega_{0,r}$  (b) from Selvam *et al.* (2009) for a miscible pseudo-interface of thickness  $\delta = 0.008$  and for weak diffusion Schmidt number,  $Sc = \mu/(\rho D_m) = 7500$ .

In the figures 7 and 8, we added the numerical results obtained by Selvam *et al.* (2009) for their smallest interface thickness  $\delta = 0.008$  and their lowest molecular diffusion, defined by the number Schmidt,  $Sc = \mu/(\rho D_m) = 7500$ . The figures show that the temporal characteristics are qualitatively similar. We however remark on the difficulty of extrapolating the numerical results due to the nonlinearity of the diffusion effect. Indeed, it has been demonstrated by Talon & Meiburg (2011) that the miscibility might contribute to an increase of the instability but that this increase varies non-monotonically with each of the two parameters  $\delta$  or  $D_m$ . The extrapolation is thus difficult to achieve as it requires us to decrease simultaneously  $\delta$  and  $D_m$  toward zero.

## 8. Conclusions

We performed a linear stability analysis of the flow of two fluids injected simultaneously and concentrically into a cylindrical tube. We have given all the details of the calculation, in particular regarding the boundary conditions, in the very general case of two immiscible fluids of different viscosity, density and inertia. First, we re-examined the creeping flow limit ( $Re = 0$ ) of two immiscible fluids and studied the transition from convective to absolute instability. We compared our results to various approximations in the literature. Then, taking advantage of C. Pekeris' elegant solution, which provides an explicit solution for the dispersion relationship of the single-fluid flow, we obtained an explicit solution for the more general case of two immiscible fluids of different viscosity, density and inertia. This formulation is well suited for implementation in commercial software. Using this complete solution, we addressed the question of the transition from convective instability to absolute instability in the case of two fluids of different viscosities but of the same density in the absence of surface tension and without diffusion (infinite Schmidt number). We studied the dependence of the convective–absolute instability transition on the Reynolds number and the location of the pseudo-interface and compared it to the available simulations.

## REFERENCES

- ABRAMOWITZ, M. & STEGUN, I. A. 1964 *Handbook of Mathematical Functions: With Formulas, Graphs, and Mathematical Tables*, vol. 55. Courier Corporation.
- BALASUBRAMANIAM, R., RASHIDNIA, N., MAXWORTHY, T. & KUANG, J. 2005 Instability of miscible interfaces in a cylindrical tube. *Phys. Fluids* **17**, 052103.
- BREVDO, L., LAURE, P. & BRIDGES, T. J. 1999 Linear pulse structure and signalling in a film flow on an inclined plane. *J. Fluid Mech.* **396**, 37–71.
- BRIGGS, R. J. 1964 *Electron-Stream Interaction with Plasma*. MIT-Press.
- CHARRU, F. & FABRE, J. 1994 Long waves at the interface between two viscous fluids. *Phys. Fluids* **6**, 1223–1235.
- CHEN, C.-Y. & MEIBURG, E. 1996 Miscible displacement in capillary tubes. Part 2. Numerical simulations. *J. Fluid Mech.* **326**, 57–67.
- CHOMAZ, J. M. 2005 Global instabilities in spatially developing flows: non-normality and nonlinearity. *Annu. Rev. Fluid Mech.* **37** (1), 357–392.
- DEISSLER, R. J. 1987 The convective nature of instability in plane Poiseuille flow. *Phys. Fluids* **30** (8), 2303–2305.
- DRAZIN, P. G. & REID, W. H. 1981 *Hydrodynamic Stability*. Cambridge University Press.
- DUPRAT, C., RUYER-QUIL, C., KALLIADASIS, S. & GIORGIUTTI-DAUPHINE, F. 2007 Absolute and convective instabilities of a viscous film flowing down a vertical fiber. *Phys. Rev. Lett.* **98**, 244502.
- GAÑÁN-CALVO, A. M., HERRADA, M. A. & GARSTECKI, P. 2006 Bubbling in unbounded coflowing liquids. *Phys. Rev. Lett.* **96** (12), 124504.
- GODRECHE, C. & MANNEVILLE, P. 1998 *Hydrodynamics and Nonlinear Instabilities*. Cambridge University Press.
- GOVINDARAJAN, R. & SAHU, K. C. 2014 Instabilities in viscosity-stratified flow. *Annu. Rev. Fluid Mech.* **46** (1), 331–353.
- GUILLOT, P., COLIN, A. & AJDARI, A. 2008 Stability of a jet in confined pressure-driven biphasic flows at low Reynolds number in various geometries. *Phys. Rev. E* **78**, 016307.
- GUILLOT, P., COLIN, A., UTADA, A. S. & AJDARI, A. 2007 Stability of a jet in confined pressure-driven biphasic flows at low Reynolds numbers. *Phys. Rev. Lett.* **99** (10), 104502.
- GUYON, E., HULIN, J.-P., PETIT, L. & DE GENNES, P. G. 2001 *Hydrodynamique Physique*. EDP sciences Les Ulis.
- HELMHOLTZ, H. 1890 Die energie der wogen und des windes. *Ann. Phys.* **41**, 641–662.
- HERRADA, M. A., GAÑÁN CALVO, A. M. & GUILLOT, P. 2008 Spatiotemporal instability of a confined capillary jet. *Phys. Rev. E* **78**, 046312.
- HICKOX, C. E. 1971 Instability due to viscosity and density stratification in axisymmetric pipe flow. *Phys. Fluids* **14**, 251–262.
- HINCH, E. J. 1984 A note on the mechanism of the instability at the interface between two shearing fluids. *J. Fluid Mech.* **144**, 463–465.
- HU, H. H. & JOSEPH, D. D. 1989 Lubricated pipelining: stability of core-annular flow. Part 2. *J. Fluid Mech.* **205**, 395–396.
- HU, X. & CUBAUD, T. 2018 Viscous wave breaking and ligament formation in microfluidic systems. *Phys. Rev. Lett.* **121**, 044502.
- HUERRE, P. & MONKEWITZ, P. A. 1990 Local and global instabilities in spatially developing flows. *Annu. Rev. Fluid Mech.* **22**, 473–537.
- JOSEPH, D. D., BAI, R., CHEN, K. P. & RENARDY, Y. Y. 1997 Core-annular flows. *Annu. Rev. Fluid Mech.* **29**, 65–90.
- JOSEPH, D. D., RENARDY, M. & RENARDY, Y. 1984 Instability of the flow of two immiscible liquids with different viscosities in a pipe. *J. Fluid Mech.* **141**, 309–317.
- JOSEPH, D. D. & RENARDY, Y. Y. 1992a *Fundamentals of Two-Fluid Dynamics. Part I: Mathematical Theory and Applications*. Springer.
- JOSEPH, D. D. & RENARDY, Y. Y. 1992b *Fundamentals of Two-Fluid Dynamics. Part II: Lubricated Transport, Drops and Miscible Liquids*. Springer.
- KELVIN, LORD 1870 Hydrokinetic solutions and observations. *Phil. Mag.* **42**, 362–377.

- KOURIS, C. & TSAMOPOULOS, J. 2001 Dynamics of axisymmetric core-annular flow in a straight tube. I. The more viscous fluid in the core, bamboo waves. *Phys. Fluids* **13**, 841–858.
- KOURIS, C. & TSAMOPOULOS, J. 2002 Dynamics of the axisymmetric core-annular flow. II. The less viscous fluid in the core, saw tooth waves. *Phys. Fluids* **14**, 1011–1029.
- KUANG, J., MAXWORTHY, T. & PETITJEANS, P. 2003 Miscible displacements between silicone oils in capillary tubes. *Eur. J. Mech. B* **22**, 271–277.
- LAJEUNESSE, E., MARTIN, J., RAKOTOMALALA, N., SALIN, D. & YORTSOS, Y. C. 1999 Miscible displacement in a Hell-Shaw cell at high rates. *J. Fluid Mech.* **398**, 299–319.
- D'OLCE, M., MARTIN, J., RAKOTOMALALA, N., SALIN, D. & TALON, L. 2008 Pearl and mushroom instability patterns in two miscible fluids core annular flow. *Phys. Fluids* **20**, 24104.
- D'OLCE, M., MARTIN, J., RAKOTOMALALA, N., SALIN, D. & TALON, L. 2009 Convective/absolute instability in miscible core-annular flow. Part 1: experiments. *J. Fluid Mech.* **618**, 305–311.
- PEKERIS, C. L. 1948 Stability of the laminar flow through a straight pipe of circular cross-section to infinitesimal disturbances which are symmetrical about the axis of the pipe. *Proc. Natl Acad. Sci.* **34** (6), 285–295.
- PETITJEANS, P. & MAXWORTHY, T. 1996 Miscible displacements in capillary tubes. Part 1. experiments. *J. Fluid Mech.* **326**, 37–56.
- RAYLEIGH, LORD 1899 On the instability of jets. *Sci. Pap.* **I**, 361–371.
- RENARDY, Y. 1987 Viscosity and density stratification in vertical Poiseuille flow. *Phys. Fluids* **30**, 1638–1648.
- SAHU, K. C., DING, H., VALLURI, P. & MATAR, O. K. 2009 Linear stability analysis and numerical simulation of miscible two-layer channel flow. *Phys. Fluids* **21**, 042104.
- SELVAM, B., MERK, S., GOVINDARAJAN, R. & MEIBURG, E. 2007 Stability of miscible core-annular flow with viscosity stratification. *J. Fluid Mech.* **592**, 23–49.
- SELVAM, B., TALON, L., LESSHAFT, L. & MEIBURG, E. 2009 Convective/absolute instability in miscible core-annular flow. Part 2: numerical simulation and nonlinear global modes. *J. Fluid Mech.* **618**, 323–348.
- SEXL, T. 1927 Zur stabilitätsfrage der poiseuilleschen und couetteschen strömung. *Ann. Phys.* **388** (14), 835–848.
- TALON, L. & MEIBURG, E. 2011 Plane Poiseuille flow of miscible layers with different viscosities: instabilities in the Stokes flow regime. *J. Fluid Mech.* **686**, 484–506.
- UTADA, A. S., FERNANDEZ-NIEVES, A., GORDILLO, J. M. & WEITZ, D. A. 2008 Absolute instability of a liquid jet in a coflowing stream. *Phys. Rev. Lett.* **100** (1), 014502.
- UTADA, A. S., FERNANDEZ-NIEVES, A., STONE, H. A. & WEITZ, D. A. 2007 Dripping to jetting transitions in coflowing liquid streams. *Phys. Rev. Lett.* **99** (9), 094502.
- YIN, X.-Y., SUN, D.-J., WEI, M.-J. & WU, J.-Z. 2000 Absolute and convective instability character of slender viscous vortices. *Phys. Fluids* **12**, 1062–1072.